It is suggested that the nitrosamine product is derived mainly from the former (eq 1), while the gaseous products arise mainly from the latter (eq 5). It is obvious that this division of products does not strictly hold. Many suggestions have been made as to how the route via N–NO_2 bond homolysis could lead to the observed gaseous products.[3-9] With some nitramines, the gases may result from subsequent decomposition of the nitrosamine, although dimethylnitrosamine is relatively stable under the thermolysis conditions. We have suggested the possibility that some nitrosamine may arise indirectly from the C–H bond scission route if the nitramine acts as the oxidizer for the carbon-containing species, oxidizing them to CO_2 and CO. Direct loss of oxygen from dimethylnitramine would form dimethylnitrosamine without allowing N–N label scrambling in the reactant nitramine; however, evidence to support this last suggestion is lacking.

Acknowledgment. We are grateful to the Office of Naval Research for their support of this work through Grant No. N00014-89-J-3143, to Dr. K. Bower for use of his high-pressure apparatus, and to R. Cohn and S. Kaushik for preliminary studies.

Registry No. DMN, 4164-28-7; DIPN, 4164-30-1; NPIP, 7119-94-0; D_2, 7782-39-0.

Reactions of C(^{1}D) with H_2 and HCl: Product State Excitations, Λ-Doublet Propensities, and Branching Ratios

D. C. Scott, J. de Juan,† D. C. Robie, D. Schwartz-Lavi, and H. Reisler*

Department of Chemistry, University of Southern California, Los Angeles, California 90089-0482
(Received: June 12, 1991; In Final Form: October 17, 1991)

The reactions of C(^{1}D) with H_2 and HCl were studied using two-photon 248-nm photolysis of C_3O_2 as the source of C(^{1}D). CH($X^2\Pi$) products were detected via LIF using the $B^2\Sigma^- \leftarrow X^2\Pi$ and $A^2\Delta \leftarrow X^2\Pi$ transitions, and conditions of no saturation and near-saturation for signals obtained using the $B^2\Sigma^- \leftarrow X^2\Pi$ transition were identified. The CH($X^2\Pi$) products are highly rotationally excited, and the Λ-doublet and spin–orbit components are equally populated in both reactions (within our experimental uncertainties). However, the CH product is the minor diatomic product in the C(^{1}D) + HCl reaction, even though the reaction channel yielding CCl has comparable exothermicity. CCl is detected by LIF via the $A^2\Delta \leftarrow X^2\Pi$ transition under near-nascent conditions and is highly vibrationally and rotationally excited. The results can be rationalized with an insertion mechanism involving short-lived carbene intermediates (i.e., CH_2, CHCl). The participation of surfaces of B_1 and A″ symmetry in the reactions with H_2 and HCl, respectively, is in accord with the observed little or no Λ-doublet preferences in the CH($X^2\Pi$) products. In general, the insertion mechanism is analogous to the mechanism of the corresponding O(^{1}D) reactions, but several low-lying states of CH_2, CHCl are likely to participate.

I. Introduction

Atomic carbon is an important reactive species which has been implicated in processes ranging from combustion to hydrocarbon synthesis.[1] Its scientific importance derives from its high reactivity and the existence of several low-lying electronic states deriving from the same $2p^2$ configuration; the ground state is 2^3P, while the 2^1D_2 and 2^1S_0 metastable states lie 1.263 and 2.684 eV, respectively, above the ground state. Despite its fundamental importance, comparatively little is known about the elementary reactions of carbon atoms under single-collision conditions and with state-resolved product detection. This is primarily due to difficulties in preparing carbon state-selectively in clean and controlled environments. Consequently, much less is known about the reactions of C(^{3}P,^{1}D) than about the corresponding reactions of O(^{3}P,^{1}D). So far, the only studies of the dynamics of C(^{1}D) involve reactions with H_2(HD, D_2).[2-4] The reactions of C(^{3}P) with HI,[5] and several oxidizers (e.g., NO,[6,7] N_2O,[7,8-10] SO_2,[11] OCS,[12] and NO_2[13,14]) have been reported, but even though some energy distributions are published, most studies (except those done in molecular beams) have been done under conditions where relaxation takes place.

Several intriguing issues concern the reactions of carbon atoms. These include, among others, the roles of abstraction and insertion, activation barriers, transition-state structure, the role of carbon spin states, and comparisons with reactions of O(^{3}P,^{1}D). In this paper, we report our findings on the reactions of C(^{1}D) with H_2 and HCl. The relevant exothermicities, excluding internal and translational energies of the reactants, are[15-17]

$$\mathrm{C(^1D) + H_2(X^1\Sigma^+) \rightarrow CH(X^2\Pi) + H(^2S_{1/2})} \qquad \Delta H = -2100\ \mathrm{cm^{-1}} \quad (1)$$

$$\mathrm{C(^1D) + HCl(X^1\Sigma^+) \rightarrow CH(X^2\Pi) + Cl(^2P_{3/2})} \qquad \Delta H = -2500\ \mathrm{cm^{-1}} \quad (2a)$$

$$\rightarrow \mathrm{CH(X^2\Pi) + Cl(^2P_{1/2})} \qquad \Delta H = -1600\ \mathrm{cm^{-1}} \quad (2b)$$

$$\rightarrow \mathrm{CCl(X^2\Pi) + H(^2S_{1/2})} \qquad \Delta H = -2000 \pm 1700\ \mathrm{cm^{-1}} \quad (2c)$$

Note the large uncertainty in the energetics of reaction 2c.

† Present address: Inasmet Centro Tecnologico de Materiales, 20009 San Sebastian, Spain.

(1) For reviews, see: (a) Mackay, C. In *Carbenes*; Moss, R. A., Jones, M., Eds.; Wiley: New York, 1975; Vol. II. (b) Shevlin, P. B. In *Reactive Intermediates*; Abramovich, R. A., Ed.; Plenum: New York, 1980; Vol. I.
(2) Jursich, G. M.; Wiesenfeld, J. R. *Chem. Phys. Lett.* **1984**, *110*, 14.
(3) Jursich, G. M.; Wiesenfeld, J. R. *J. Chem. Phys.* **1985**, *83*, 910.
(4) Fisher, W. H.; Carrington, T.; Sadowski, C. M.; Dugan, C. H. *Chem. Phys.* **1985**, *97*, 433.
(5) Nishiyama, N.; Sekiya, H.; Nishimura, Y. *J. Chem. Phys.* **1986**, *84*, 5213.
(6) (a) Jackson, W. M.; Beugre, C. N.; Halpern, J. B. *J. Photochem.* **1980**, *13*, 319. (b) Krause, H. F. *Chem. Phys. Lett.* **1981**, *78*, 78. (c) Sekiya, H.; Tsuji, M.; Nishimura, Y. *J. Chem. Phys.* **1986**, *84*, 3739.
(7) (a) Costes, M.; Naulin, C.; Dorthe, G.; Houdden, Z. *Laser Chem.* **1990**, *10*, 367. (b) Costes, M.; Naulin, C.; Dorthe, G. *Astron. Astrophys.* **1990**, *232*, 270.
(8) (a) Dorthe, G.; Costes, M.; Destriau, M. *J. Photochem.* **1978**, *9*, 168. (b) Costes, M.; Dorthe, G.; Caubet, Ph. *J. Chem. Phys.* **1981**, *74*, 6523. (c) Dorthe, G.; Joussot-Dubien, J.; Nouchi, G.; Kottis, Ph. *Laser Chem.* **1983**, *2*, 373. (d) Costes, M.; Dorthe, G.; Destriau, M. *Chem. Phys. Lett.* **1979**, *61*, 588.

0022-3654/92/2096-2509$03.00/0

Since HCl dissociates at wavelengths where C_3O_2 forms $C(^1D)$ in single-photon dissociation (e.g., 157 nm),[15] the source of $C(^1D)$ employed in this study is two-photon 248-nm photolysis of C_3O_2. The 248-nm photolysis of C_3O_2 has not been used before as a source of $C(^1D)$, and therefore we have reexamined reaction 1, paying special attention to the Λ-doublet populations in the CH($X^2\Pi$) product. A previous report of these populations was preliminary and did not provide a detailed explanation of the observed propensities.[3] In this work, we detect CH via both the $B^2\Sigma^- \leftarrow X^2\Pi$ and $A^2\Delta \leftarrow X^2\Pi$ transitions and conclude that there is no significant Λ-doublet preference in reactions 1 and 2 for $N = 2$–12. This is rationalized as indicating the participation of CH_2 and CHCl reactive intermediates of both $A_1(A')$ and $B_1(A'')$ symmetry.

Reaction 2 is of particular interest because it has three channels of comparable exothermicity, and thus can serve as an indicator for the importance of statistics vs dynamics. In addition, it can be compared to the corresponding $O(^1D)$ + HCl reaction, which has been studied extensively.[18,19] We find that CCl is the dominant product and that both CH and CCl are highly internally excited. Again, no significant Λ-doublet preference in CH is observed.

II. Experimental Section

The experimental arrangement was similar to the one used before,[20] and typical of pump/probe measurements using pulsed laser sources. Carbon atoms were produced by two-photon 248-nm photolysis of carbon suboxide (C_3O_2). The photodissociation of C_3O_2 in the 248-nm band has only recently been studied in detail,[21-24] and is known to generate $C(^1D)$.[23,24] A KrF excimer laser (Lambda Physik EMG 50 or Questek 2220M) was used to generate 50–150 mJ of 248-nm radiation which was focused into the reaction chamber by a 50-cm lens. Premixed samples of 10–30% C_3O_2 in H_2 or HCl were used in these experiments. The samples flowed slowly at total pressures 25–100 mTorr and were replenished between laser firings. In order to avoid complications from possible slow dark reactions, a fresh mix was prepared daily.

CH was detected via laser-induced fluorescence (LIF) using either the $B^2\Sigma^- \leftarrow X^2\Pi$ or $A^2\Delta \leftarrow X^2\Pi$ transitions. Both are well characterized in the literature, and line positions and line strengths were determined using standard procedures and published constants.[25] The B ← X system is easier to analyze than the A ← X system because it has fewer branches; however, predissociation is known to occur in the $B^2\Sigma^-$ state of CH beginning with $N' = 17$. The main advantage of using the A ← X system is that both Λ-doublet and spin–orbit populations can be derived from the same rotational branch line and thus saturation does not affect the populations (see below). The A ← X system is not predissociative but is more complex and prone to rotational-line overlaps.[25] Also, the two-photon 248-nm photodissociation of C_3O_2 produces fluorescence at 430 nm (coinciding with the A ← X LIF) whose intensity is comparable to the CH LIF signals at short (<0.5 μs) delays. This problem is particularly severe in the C + HCl experiments, where the CH LIF signals are very small. The C_3O_2 fluorescence at 390 nm, which coincides with the B ← X fluorescence, is much smaller. CCl was detected via LIF using the $A^2\Delta \leftarrow X^2\Pi$ $\Delta v = 0$ sequence around 278 nm.[26-28] Some lines of the $\Delta v = -1$ and $\Delta v = -2$ sequences were also detected. Although some uncertainties still exist in the spectral assignments of the CCl A ← X system, it appears that the $v' \geq 1$ states are predissociative.[27] Further discussion of CCl spectroscopy is given in section III. The excimer-pumped dye laser used to probe the products (Lambda Physik EMG 50 + Lumonics EPD 330 or Lambda Physik MSC 201 + FL3002) was fired 0.2–100 μs after the photolysis laser. For CCl detection, the laser output was frequency doubled using a KDP crystal. The two laser beams were either parallel and counterpropagating, or perpendicular. The diameter of the probe beam was 2–3 mm.

LIF was detected through interference filters, 279.0 ± 5.5 nm (Corion) for CCl, 385 ± 11 nm (Corion) for CH B ← X, and 425 ± 25 nm (Omega) for CH A ← X. The GaAs photomultiplier tube (PMT, Hamamatsu R943-02) was mounted at right angles to the laser beams. Signals from the PMT were recorded using a digital oscilloscope (Nicolet, Explorer III) interfaced to a computer (LSI 11/23), which controlled the experiment and normalized the signals with respect to the probe laser intensity variations. Typically, signals from 10 to 30 laser firings were averaged for each data point. Relative laser pulse energies were measured with a photodiode (United Detector Technology, UDT-UV005), while absolute pulse energies were measured with power meters (Scientech 380105 and Molectron J3-05 for high and low energies, respectively). The pulse energy measurements were particularly important in determining whether the LIF measurements were done under saturation conditions. For these experiments, the photodiode readings were calibrated relative to the absolute energy readings, so that measurements spanning ~2 orders of magnitude of probe laser energy could be carried out. The CCl LIF signals were usually large and these LIF measurements were performed in the linear regime, prior to the onset of saturation. Since the CH LIF signals from reaction 2 were small, the measurements of all CH LIF spectra were performed under conditions of almost complete saturation. More details of the data analyses are given in section III.

In order to measure products under single-collision conditions and to minimize relaxation, it was necessary to work at low gas densities and short delays. In typical experiments, total pressures of 25–70 mTorr and delays of 0.2–1 μs between the photolysis and probe lasers were used. Shorter delays could not be used because of the decrease in signal level and interference from prompt fluorescence arising from C_3O_2 photolysis.

Carbon suboxide was prepared by dehydration of malonic acid following the method of Long et al.,[29,30] as modified by Strauss et al.[31] Purification from the main impurity, CO_2, was achieved by pumping on the sample at −105 °C (ethanol slush). HCl (Matheson, >99.5%) and H_2 (Matheson 99.995%) were used without further purification.

III. Results

1. Saturation Measurements in the CH($B^2\Sigma^- \leftarrow X^2\Pi$) System. To determine the Λ-doublet propensities in the CH product of

(9) Dorthe, G.; Costes, M.; Naulin, C.; Joussot-Dubien, J.; Vaucamps, C.; Nouchi, G. *J. Chem. Phys.* **1985**, *83*, 3171.
(10) Torchin, L.; Bordas, M. C.; Robert, J. C. *Appl. Phys. Lett.* **1985**, *47*, 660.
(11) (a) Dorthe, G.; Costes, M.; Burdenski, S.; Caille, J.; Caubet, Ph. *Chem. Phys. Lett.* **1983**, *94*, 404. (b) Krause, H. F. *Chem. Phys. Lett.* **1981**, *83*, 165.
(12) Dorthe, G.; Caille, J.; Burdenski, S. *J. Chem. Phys.* **1983**, *78*, 594.
(13) Dorthe, G.; Caille, J.; Burdenski, S.; Caubet, P.; Costes, M.; Nouchi, G. *J. Chem. Phys.* **1985**, *82*, 2313.
(14) Sekiya, H.; Tsuji, M.; Nishimura, Y. *J. Chem. Phys.* **1985**, *83*, 2857.
(15) Okabe, H. *Photochemistry of Small Molecules*; Wiley: New York, 1978.
(16) Benson, S. W. *Thermochemical Kinetics*; Wiley: New York, 1976.
(17) Chase, M. W. Jr.; Davies, C. A.; Downey, J. R. Jr.; Frurip, D. J.; McDonald, R. A.; Syverud, A. N. JANAF Thermochemical Tables, Third Edition Part I. *J. Phys. Chem. Ref. Data* **1985**, *14*, Suppl. 1.
(18) Kruus, E. M.; Niefer, B. I.; Sloan, J. J. *J. Chem. Phys.* **1988**, *88*, 985.
(19) Park, C. R.; Wiesenfeld, J. R. *Chem. Phys. Lett.* **1989**, *163*, 230.
(20) (a) Qian, C. X. W.; Noble, M.; Nadler, I.; Reisler, H.; Wittig, C. *J. Chem. Phys.* **1985**, *83*, 5573. (b) de Juan, J.; Callister, S.; Reisler, H.; Segal, G. A.; Wittig, C. *Ibid.* **1988**, *89*, 1977.
(21) McFarlane, J.; Polanyi, J. C.; Shapler, J. G.; Williamson, J. M. *J. Photochem. Photobiol. A* **1989**, *46*, 139.
(22) Anderson, D. J.; Rosenfeld, R. N. *J. Chem. Phys.* **1991**, *94*, 7857.
(23) Umemoto, M.; Shinohara, H.; Nishi, N. *J. Photochem.* **1982**, *20*, 277.
(24) Das, P.; Ondrey, G.; van Veen, N.; Bersohn, R. *J. Chem. Phys.* **1983**, *79*, 724.
(25) (a) Moore, C. E.; Broida, H. P. *J. Res. Natl. Bur. Stand.* **1959**, *63A*, 19. (b) Gerö, L. *Z. Phys.* **1941**, *118*, 27.
(26) (a) Verma, R. D.; Mulliken, R. S. *J. Mol. Spectrosc.* **1961**, *6*, 419. (b) Gordon, R. D.; King, G. W. *Can. J. Phys.* **1961**, 39, 252. (c) Merer, A. J.; Travis, D. N.; Watson, J. K. G. *Can. J. Phys.* **1966**, *44*, 447.
(27) Larsson, M.; Blomberg, M.; Siegbahn, P. *Mol. Phys.* **1982**, *46*, 365.
(28) Mélen, F.; Houbrechts, Y.; Dubois, I.; Bredohl, H. *J. Phys. B: At. Mol. Phys.* **1983**, *16*, 2523.
(29) Long, D. A.; Murfin, F. S.; Williams, R. L. *Proc. R. Soc. London, Ser. A* **1954**, *223*, 251.
(30) Miller, F. A.; Fateley, W. G. *Spectrochim. Acta* **1964**, *20*, 253.
(31) Strauss, C. E. M.; Kable, S. H.; Chawla, G. K.; Houston, P. L.; Burak, I. R. *J. Chem. Phys.* **1991**, *94*, 1837.

reactions 1 and 2, a quantitative comparison between the rotational level populations determined by Q vs P and R branch lines of the $B^2\Sigma^- \leftarrow X^2\Pi$ transition is necessary. The relation between the observed line intensities and level populations depends on the extent of saturation.[32,33] Assuming constant laser intensity and neglecting polarization, quenching and weak frequency dependences, in a $^2\Sigma^-$–$^2\Pi$ transition

$$\frac{n[J'',\Pi(A'')]}{n[J'',\Pi(A')]} = C\frac{I_{P,R}(J'')}{I_Q(J'')} \qquad (3)$$

where $n[J'',\Pi(A'',A')]$ is the population of the $\Pi(A'')$ or $\Pi(A')$ Λ-doublet components of the J'' rotational level. $I_{P,R}(J'')$ is the intensity of the $P(J'')$ or $R(J'')$ line, $I_Q(J'')$ is the intensity of the $Q(J'')$ line, and

$$C = \frac{S_Q(J'',J'_Q)}{S_{PR}(J'',J'_{PR})} \quad \text{(unsaturated)} \qquad (4a)$$

$$= \frac{1}{2}\left(\frac{2J''+1}{2J'_{PR}+1} + 1\right) \quad \text{(saturated)} \qquad (4b)$$

$S(J'',J')$ is the appropriate Hönl–London factor.[34] Recall that $J'' = N'' + {}^1/_2$ and $N'' - {}^1/_2$ for F_1 and F_2 states, respectively. In the limit of high J'', the coefficients in eq 4 differ by a factor of 2. Experimental considerations favor the use of the $B^2\Sigma^- \leftarrow X^2\Pi$ transition for CH LIF detection as described above; however, Fisher et al. were not able to obtain reliable Λ-doublet populations via this transition, even for thermalized samples where the two Λ-doublet components of $CH(X^2\Pi)$ are equally populated.[4] Under experimental conditions similar to ours, these authors placed the onset of saturation at pulse energies of 125 μJ and used energies of 15–75 μJ/pulse when obtaining CH LIF spectra.

In our experiments, we also observed anomalous Λ-doublet populations when using comparable probe laser energies. We therefore rechecked carefully for the onset of saturation using laser pulse energies $\geq$0.5 μJ/pulse (pulse duration $\sim$ 10 ns fwhm; bandwidth 0.12 cm^{-1}). In these experiments CH was prepared by two-photon photolysis of CH_3I at 248 nm and thermalized in 0.9 Torr of Xe. At pump/probe delays $\geq$ 10 μs, the measured CH rotational and spin–orbit temperatures were 300 K. We used two criteria in determining the onset of saturation: deviations from linearity in a plot of CH LIF signal vs laser pulse energy, and changes in the intensity ratios of Q to P,R branch lines with increasing laser pulse energies. Figure 1 is a plot of CH LIF signals vs laser pulse energies. At laser intensities $\leq$4 kW cm^{-2} ($\leq$3 μJ/pulse) the slope was 0.98 $\pm$ 0.06, as expected for unsaturated conditions [see Figure 1b]. At these intensities, rotational level populations derived from the relative intensities of P, Q, or R branch lines assuming no saturation (eq 4a) agreed within experimental errors. When the pulse energy exceeded 3 μJ, deviations from linearity were observed as shown in Figure 1a, and relative populations calculated assuming no saturation showed an apparent preference for the $\Pi(A'')$ state. This indicates the onset of saturation. At pulse energies $\geq$30 μJ, the ratio $n[J'',\Pi(A'')]/n[J'',\Pi(A')]$ varied only slowly with laser pulse energy, indicating that near-saturation conditions were reached. Assuming complete saturation at this point (eq 4b) yielded a ratio slightly less than unity. The small deviation from unity ($\sim$10–15%) is possibly caused by residual polarization and saturation effects or other instrumental biases. We conclude that under our experimental conditions the saturation onset for the CH $B^2\Sigma^- \leftarrow X^2\Pi$ transition is $\sim$3 μJ. Thus, when saturation effects are properly taken into account, the B $\leftarrow$ X system can be used to obtain both rotational populations and Λ-doublet propensities.

2. Rotational Distributions and Branching Ratios. (a) CH Rotational Distributions. The rotational distributions of $CH(X^2\Pi,v''=0)$ from reactions 1 and 2 were determined from LIF

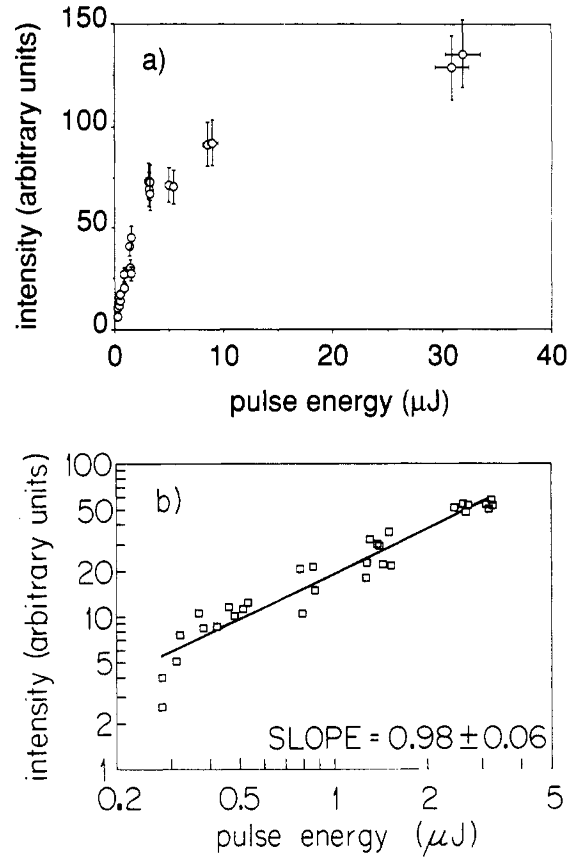

Figure 1. Dependence of the $CH(B^2\Sigma^- \leftarrow X^2\Pi)$ LIF signals on the probe-laser pulse energy. The laser pulse duration and bandwidth were 10 ns and 0.12 cm^{-1}, respectively. (a) Linear plot that shows distinct deviations from linearity at pulse energies > 3 μJ; (b) log–log plot showing a slope of 1 at energies <3 μJ.

spectra of the $B^2\Sigma^- \leftarrow X^2\Pi$ system. The $A^2\Delta \leftarrow X^2\Pi$ system was used in some of the experiments. Rotational level populations of the two spin-orbit states, $^2\Pi_{1/2}$ and $^2\Pi_{3/2}$, were determined from Q, R, and P lines, using eqs 3 and 4b. The best S/N ratios at the shortest photolysis/probe time delays were achieved at high probe-laser intensities where near-saturation conditions prevailed, and these conditions were used in obtaining the spectra. Figures 2 and 3 display typical CH spectra obtained via the B $\leftarrow$ X and A $\leftarrow$ X systems, respectively. Spectral assignments were done by comparisons with published line positions,[25,35] and by using spectral simulations.[36] Figure 2 shows a portion of the CH spectrum obtained in reaction 2, while in Figure 3, the R(8) and R(9) lines of the CH A $\leftarrow$ X spectrum obtained in reaction 1 are displayed. Here, both the spin–orbit and Λ-doublet components are well resolved, and it is apparent that the two Λ-doublet components are nearly equally populated, as discussed in more detail in section III.3.

Relative $CH(X^2\Pi,v''=0)$ rotational populations, $n(N'')$, were derived from measured peak heights or areas of the B $\leftarrow$ X transition assuming saturation and using

$$n(N'') = KI(N'')(g'' + g')/g' \qquad (5)$$

where $I(N'')$ is the rotational line intensity corrected for PMT and filter responses, g' and g'' are the rotational degeneracies of the upper and lower states, respectively, and K is an instrumental factor. As discussed above, even at high probe laser energies and thermalized samples, the ratios $n[N'',\Pi(A'')]/n[N'',\Pi(A')]$ were slightly smaller than unity. On the other hand, data obtained via the CH A $\leftarrow$ X system showed conclusively that the two Λ-doublet components of $CH(X^2\Pi)$ were equally populated (see below), and thus we expected P, Q, and R branch lines to yield identical

(32) Altkorn, R.; Zare, R. N. *Annu. Rev. Phys. Chem.* **1984**, *35*, 265.
(33) Macdonald, R. G.; Liu, K. *J. Chem. Phys.* **1989**, *91*, 821.
(34) Kovacs, I. *Rotational Structure in the Spectra of Diatomic Molecules*; American Elsevier: New York, 1969.
(35) Herzberg, G.; Johns, J. W. C. *Astrophys. J.* **1969**, *158*, 399.
(36) Huber, K. P.; Herzberg, G. *Constants of Diatomic Molecules*; Van Nostrand: New York, 1979.

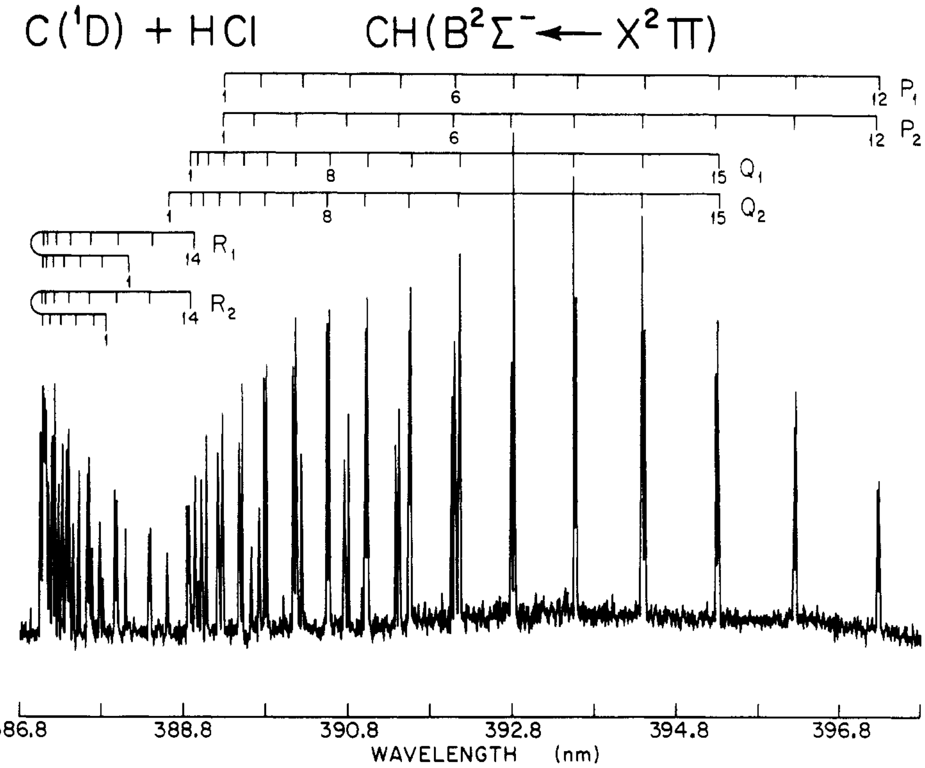

Figure 2. Part of the LIF $CH(B^2\Sigma^- \leftarrow X^2\Pi)$ (0,0) spectrum obtained from reaction 2. 50 mTorr of sample (C_3O_2:HCl = 1:9) was photolyzed at 248 nm. The delay between the photolysis and probe pulses was 0.5 μs.

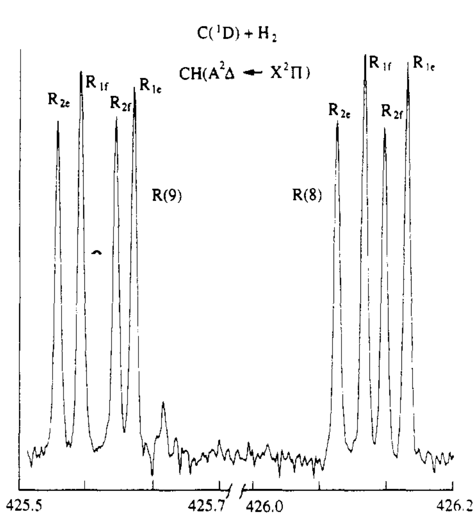

Figure 3. The R(8) and R(9) lines of the LIF $CH(A^2\Delta \rightarrow X^2\Pi)$ (0,0) transition obtained from reaction 1. The subscripts 1 and 2 denote the $^2\Pi_{1/2}$ and $^2\Pi_{3/2}$ spin–orbit states, while e and f denote the Λ-doublet components. The two Λ-doublet components of each spin–orbit state are equally populated. Even though the R_1 lines are stronger than R_2 lines, they correspond to equal populations of the $^2\Pi_{1/2}$ and $^2\Pi_{3/2}$ spin–orbit states. The experimental conditions were similar to those of Figure 1, with H_2 replacing HCl. 25 mTorr of sample (C_3O_2:HCl = 1:9) was photolyzed, and the delay between the photolysis and probe pulses was 0.5 μs.

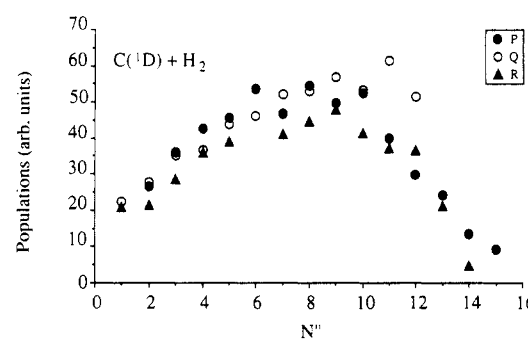

Figure 4. $CH(X^2\Pi, v=0)$ rotational populations obtained in reaction 1. The rotational level populations obtained from Q, P, and R lines were normalized as described in the text, and populations derived from the two spin–orbit states were averaged for each branch. The experimental conditions were similar to those of Figures 2 and 3.

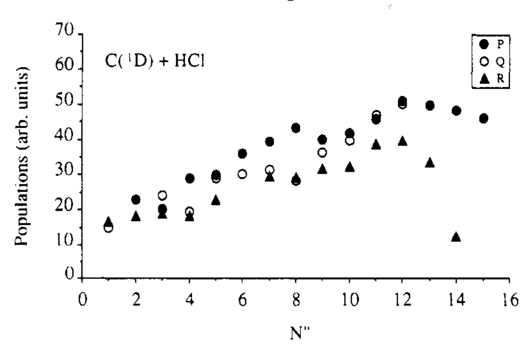

Figure 5. $CH(X^2\Pi, v=0)$ rotational populations obtained via reaction 2. The experimental conditions were similar to those of Figures 2 and 3.

populations. Since we do not know the exact origin of the small discrepancy between measurements done with the two transitions, we have employed a single "instrumental" factor to bring the populations obtained from P, R, and Q branch lines of the B ← X transition into better agreement. This factor is the ratio of the average $I_R(^2\Pi_{3/2},e)/I_R(^2\Pi_{3/2},f)$ value measured for R(8) and R(9) via the A ← X transition (Figure 3), and the ratio $n[N'',\Pi(A'')]/n[N'',\Pi(A')]$ determined for $CH(N''=8,9)$ via the B ← X transition from reaction 1. We obtained $K = 1.13 \pm 0.09$ for P and R lines and this value was used in analyzing all the CH rotational distributions and Λ-doublet populations obtained in reactions 1 and 2. The populations obtained from the P, Q, and R branch lines of the B ← X transition analyzed in this way are displayed in Figures 4 and 5 for CH obtained in reactions 1 and 2, respectively. We emphasize that the shape of the rotational distribution does not change when the correction factor is used; its only effect is to bring the absolute *intensities* of Q and P/R lines into better agreement. In these experiments, 50 mTorr samples (1:9 C_3O_2:HX) were used with 0.5 μs pump/probe delays.

Notice that according to the exothermicities listed above, rotational levels up to $N'' = 11$ and 12 are allowed for reactions 1 and 2a, respectively. The rotational populations beyond these values must result from the internal and translational energy of the reactants, or from other reactive processes. The CH($^2\Pi$) spin–orbit populations were determined from the line intensities by using appropriate line strengths, taking into account that $N'' = J'' - ^1/_2$ and $J'' + ^1/_2$ for F_1 and F_2 states, respectively. No spin–orbit preference was obtained when using either the A $\leftarrow$ X or B $\leftarrow$ X transitions. Thus, in Figures 4 and 5 the populations derived from the F_1 and F_2 components of each N'' level were averaged.

The excess energy available to the fragments following two-photon dissociation of C_3O_2 at 248 nm is 22 300 cm^{-1}, using D_0 = 58 400 cm^{-1} as the dissociation energy for $C_3O_2 \rightarrow 2CO(X^1\Sigma) + C(^1D)$.[15,17,37] If all the excess energy appears in C(^{1}D) translation, then the relative energies in the c.m. system for the C(^{1}D) reactions with H_2 and HCl are $\leq$2600 and 13 800 cm^{-1}, respectively. These values are upper limits, and the actual values are probably much lower (see section IV). Thus, the translational energy may contribute to the population of the high rotational levels of CH. CH distributions determined upon addition of 1 Torr of Ne or Ar while keeping other experimental conditions constant did not show a significant change in the populations of high N'' levels both for reactions 1 and 2, even though the reactants are expected to be translationally cooled.[2,4] The results for reaction 1 are in good agreement with those obtained by Fisher et al.[4] and by Jursich and Wiesenfeld[2] following photolysis at 157 nm. The latter authors also showed that the CH rotational distribution is well fit by a prior distribution that includes the thermal energy of H_2.[2] Thus, for reaction 1 it appears that the main contribution to high N'' beyond the thermochemical limit is the thermal energy of H_2.

The situation is more complex for reactions 2a and 2b. It is hard to reconcile the observed high N'' results with contributions from the thermal energy of HCl alone, since the high N'' CH populations do not show a gradual decrease beyond the thermochemical limit. In fact, the abrupt decrease at $N'' > 16$ is caused by $v' = 1$ predissociation. Measurements done with the A $\leftarrow$ X system, which is not predissociative, definitely showed rotational population at $N'' > 16$. However, due to the small CH signals and interference from prompt fluorescence at short pump/probe time delays, no quantitative information could be obtained. Therefore, a second experiment was conducted to check whether reaction 2 is the main source of CH. C(^{1}D) was quenched by adding Xe at pressures of 0.5–1.0 Torr, in order to determine if the high CH rotational levels derive from reaction 2. The quenching of C(^{1}D) by Xe is fast ($k = 1.1 \pm 0.3 \times 10^{-10}$ cm^3 molecule^{-1} s^{-1}) and comparable to the removal rate of C(^{1}D) by H_2 ($k = 2.6 \pm 0.3 \times 10^{-10}$ cm^3 molecule^{-1} s^{-1}).[37] We observed a substantial decrease in the CH product from reaction 1, as expected from the relative pressures of H_2 and Xe and the published rates. However, the high N'' levels of CH obtained in the HCl reaction did not decrease significantly upon the addition of Xe. We thus suspect that the high N'' levels are partially populated via another reaction. We note that, even in reaction 1, the high N'' levels decreased in intensity somewhat less than the low N'' levels. Due to the much lower signal levels from reaction 2a as compared with reaction 1, contaminations from side reactions may be more severe, affecting especially $N'' > 12$. Thus, we suspect that sources other than reaction 2 possibly contribute to the CH high rotational levels, and these are discussed in section IV.

As stated above, the CH signals from reaction 2 are much lower than those obtained from reaction 1. A quantitative comparison shows that when equal pressures and delays are used [CH(H_2)]/[CH(HCl)] $\approx$ 7, but since the CH detected in studying reaction 2 possibly includes some contributions from other reactions, we view this value as a lower limit. We do not know what is the source of the highly rotationally excited CH($X^2\Pi$) which is not quenched effectively by Xe. We rule out excited metastable C_2O and C(^{1}S), which would have been quenched, but since the CH signal from reaction 2 is so small, we cannot rule out unknown contaminations in HCl or C_3O_2, or even radical–radical reactions.

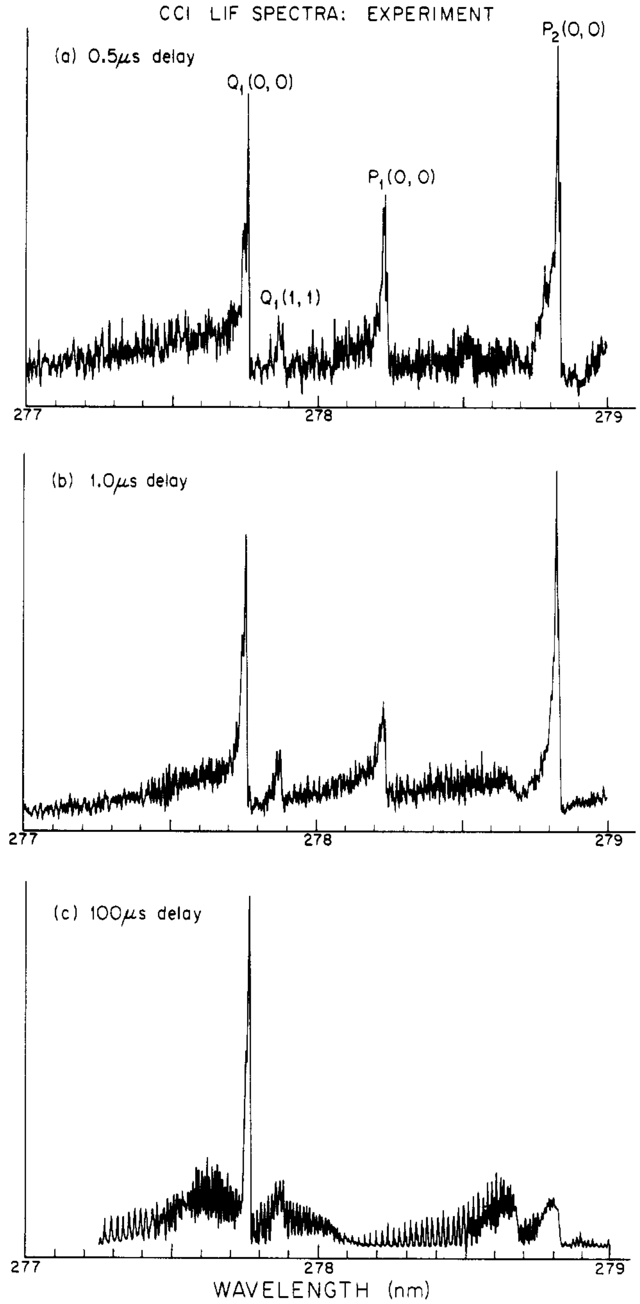

Figure 6. CCl($A^2\Delta \leftarrow X^2\Pi$) $\Delta v = 0$ LIF spectrum obtained upon photolysis of C_3O_2:HCl mixtures at 248 nm, using pump–probe delays of (a) 0.5 μs; (b) 1.0 μs, and (c) 100.0 μs. Notice that the (0,0) P_1 bandhead decreases strongly with increasing delay. Part c corresponds to a fully relaxed rotational spectrum. Other experimental details are given in the text.

(b) CCl Excitation. Since the CH signals obtained from reaction 2 were small, we looked for CCl via the $A^2\Delta \leftarrow X^2\Pi$ transition. In Figure 6a, we show a spectrum of the $\Delta v = 0$ sequence obtained at 45 mTorr total pressure (C_3O_2:HCl = 1:8) and 0.5 μs pump/probe delay. The same spectral region is displayed in Figure 6b, with 70 mTorr of 1:3 C_3O_2:HCl and 1.0 μs delay; and in Figure 6c, with 70 mTorr of 1:8 C_3O_2:HCl and 100 μs delay. The extensive rotational relaxation at longer delay times and higher pressures is evident. The spectrum was assigned using simulations of the A $\leftarrow$ X transition with published spectroscopic constants.[28,39] A simulated spectrum using N'' = 1–100 and

(37) Filseth, S. W. *Adv. Photochem.* **1977**, *10*, 1.
(38) Husain, D.; Norris, P. E. *Faraday Discuss. Chem. Soc.* **1979**, *67*, 273.
(39) Sharpe, S. W.; Johnson, P. M. *J. Mol. Spectrosc.* **1986**, *116*, 247.

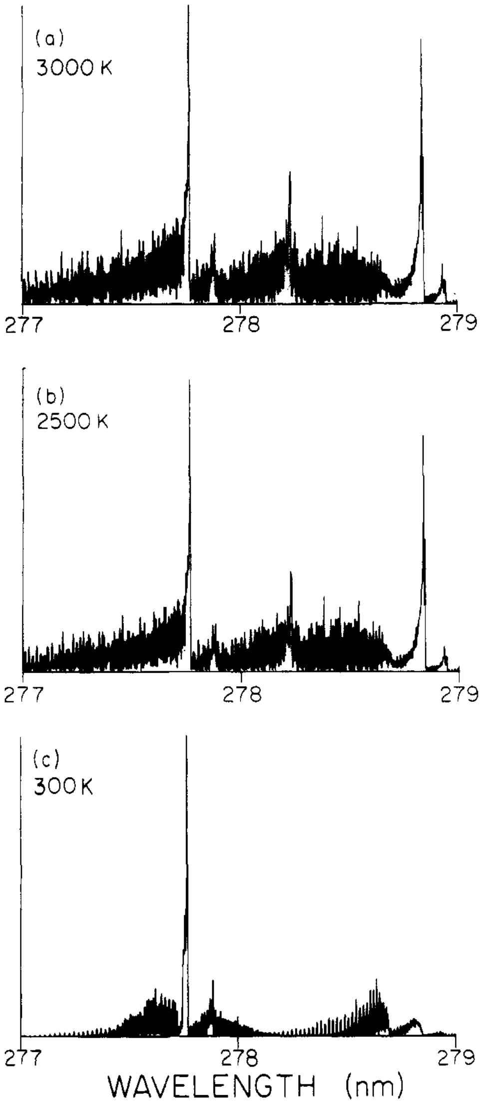

Figure 7. Simulated $CCl(A^2\Delta \leftarrow X^2\Pi)$ $\Delta v = 0$ spectra, obtained using formulas given in ref 28, and spectroscopic constants given in ref 41. The simulations assume $n(v''=1):n(v''=0) = 3:4$ and take into consideration the different lifetimes of $CCl(A^2\Delta)$ $v' = 0$ and 1.

assuming a rotational and spin-orbit temperature of 3000 K within the $v'' = 0$ and 1 vibrational levels is shown in Figure 7a. The Q_1, P_1, and P_2 bandheads of the (0,0) band and the Q_1 bandhead of the (1,1) band are all evident. The (0,0) P_1 bandhead was assigned by some previous workers as the (2,2) Q_1 bandhead,[27,40] but we have recently shown that this assignment is incorrect.[41] The (0,0) P_1 bandhead is formed at $N'' > 45$, or $E_{rot} > 1400$ cm^{-1}. As expected, this bandhead decreases markedly at 2500 K [Figure 7b], and disappears at 300 K [Figure 7c]. Clearly, the spectrum of CCl obtained at short pump/probe delays exhibits high rotational excitation. The simulations most closely match the experimental spectra when the CCl rotational temperatures are 2500–3500 K, yielding $E_{rot} = 1700$–2500 cm^{-1}. Therefore, a large fraction of the available energy of reaction 2 appears as rotational excitation.

The upper $A^2\Delta$ state of CCl is predissociative, and the measured lifetimes of the $A^2\Delta$ $v' = 1$ spin-orbit states are 35.0 ± 1.0 and 17.4 ± 0.9 ns for F_1 and F_2, respectively.[27] These lifetimes are shorter than the 108.2 ± 2 ns lifetime measured for both spin-orbit components of $v' = 0$.[27] The spectral simulations show good agreement with the experimental data when assuming that the ratio of the (1,1) to (0,0) band is ~0.3. Assuming the same

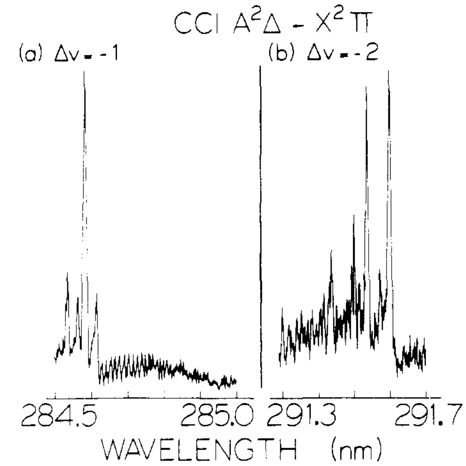

Figure 8. $CCl(A^2\Delta \leftarrow X^2\Pi)$ LIF spectra obtained in the region of the (a) $\Delta v = -1$ and (b) $\Delta v = -2$ sequences. The bandheads in (a) correspond to the (0,1) and (1,2) transitions, while those in part b correspond to the (0,2) and (1,3) transitions. The assignments are based on the $C^{35}Cl$ bandheads given in ref 28.

Franck–Condon factors for the (0,0) and (1,1) bands,[26] and correcting for the lifetime differences,[27] we estimate that about twice as many CCl molecules are formed in $v'' = 0$ as in $v'' = 1$. Thus, substantial vibrational excitation is manifest in CCl. Our simulations show that the (2,2) band is strongly overlapped by other bands in the $\Delta v = 0$ sequence, so the production of CCl in $v'' = 2$ cannot be estimated from the $\Delta v = 0$ sequence. We therefore looked for LIF signals in the spectral region of the $\Delta v = -1$ and $\Delta v = -2$ sequences. Because the internuclear distances and vibrational constants of CCl in the $X^2\Pi$ and $A^2\Delta$ states are similar,[26,39] we anticipated poor Franck–Condon factors for the $\Delta v < 0$ sequences. Indeed, the signals were small and LIF spectra with good S/N could be obtained only at long delays (≥8 μs), where the rotational distributions are already relaxed. Nevertheless, Figure 8 clearly shows peaks that may be assigned to the Q_1 bandheads of the (0,1), (1,2), (0,2), and (1,3) bands, whose published bandheads for $C^{35}Cl$ are at 35 128.2, 35 124.6, 34 284.3, and 34 293.3 cm^{-1}, respectively.[27] The relative populations of the higher vibrational levels cannot be determined quantitatively, because good spectroscopic constants are unavailable. However, from the spectra displayed in Figure 8, it appears that $n(v''=1) > n(v''=2)$ and $n(v''=2) \approx n(v''=3)$.

3. $CH(X^2\Pi)$ Λ-Doublet Populations. In the limit of Hund's case (b), the populations of the Λ-doublet components of electronic states of radicals in Π states yield information on the preferential orientation of the singly occupied π-orbital with respect to the plane of rotation of the diatom.[42,43] For reactions proceeding via a triatomic intermediate, the Λ-doublet propensities may indicate whether the unpaired electron originates from an in-plane, Π(A′), or out-of-plane, Π(A″), orbital in the transition state.[42,43] $CH(X^2\Pi)$ reaches the Hund's case (b) limit for $N'' \sim 2$,[42] and therefore, Λ-doublet propensities can be easily identified. In the reactions of $O(^1D)$ with H_2 and HCl significant preference for the in-plane Λ-doublet component was observed and interpreted as an indication that the reaction proceeds via the ground $H_2O(\tilde{X}^1A_1)$ surface.[19,44] Λ-doublet propensities have been measured for reaction 1 via the $CH(A \leftarrow X)$ system and a preference for the in-plane component was observed for $N'' > 8$.[3] Because of spectral congestion, measurements below $N'' < 4$ could not be done.

We have determined the Λ-doublet propensities for reaction 1 by using both the $B^2\Sigma^- \leftarrow X^2\Pi$ and $A^2\Delta \leftarrow X^2\Pi$ systems, which enabled us to determine the population of the two $CH(X^2\Pi)$ Λ-doublet components for $N'' = 2$–12. The $A \leftarrow X$ system yields the most direct measurement. For many rotational levels of

(40) Breitbarth, F.-W.; Berg, D.; Tiller, H.-J. *Chem. Phys. Lett.* **1987**, *135*, 435.
(41) Robie, D. C.; de Juan, J.; Reisler, H. *J. Mol. Spectrosc.* **1991**, *150*, 296.
(42) Andresen, P.; Rothe, E. W. *J. Chem. Phys.* **1985**, *82*, 3634.
(43) Alexander, M. H., et al. *J. Chem. Phys.* **1988**, *89*, 1749.
(44) (a) Butler, J. E.; Jursich, G. M.; Watson, I. A.; Wiesenfeld, J. R. *J. Chem. Phys.* **1986**, *84*, 5363. (b) Sears, T. J.; Hall, G. E.; McAndrew, J. J. F. *Ibid.* **1989**, *91*, 5201.

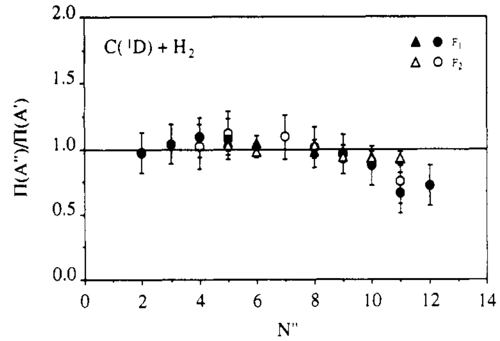

Figure 9. Λ-doublet population ratios obtained in the C(^{1}D) + H_2 reaction. $\Pi(A')$ and $\Pi(A'')$ correspond to cases where the singly occupied π electron in CH is oriented in the plane and perpendicular to the plane of rotation, respectively. Filled and empty symbols correspond to the $^2\Pi_{1/2}$ and $^2\Pi_{3/2}$ spin-orbit components, respectively. Circles and triangles give the ratios obtained via the $B^2\Sigma^- \leftarrow X^2\Pi$ and $A^2\Delta \leftarrow X^2\Pi$ transitions, respectively.

TABLE I: CH Λ-Doublet Population Ratios $\Pi(A'')/\Pi(A')$[a]

	$B^2\Sigma^-$–$X^2\Pi$[b]		$A^2\Delta$–$X^2\Pi$	
N''	F_1	F_2	F_1	F_2
2	0.97			
3	1.04			
4	1.09	1.02		
5	1.08	1.12	1.05	1.03
6			1.05	0.98
7		1.09		
8	1.01		0.98	1.02
9	0.96		0.98	0.94
10	0.87		0.94	0.93
11	0.66	0.75	0.92	0.93
12	0.72			

[a] The experimental error is ±15%. [b] A correction factor of 1.13 was applied to these data as explained in the text.

CH($X^2\Pi$), the Λ-doublets, as well as the spin-orbit components of each branch line, are well separated (see Figure 3). Thus, the Λ-doublet and spin-orbit propensities can sometimes be obtained from a single branch line and therefore are immune to saturation effects. The spectral assignments were obtained from ref 25, and the results yield $\Pi(A'')/\Pi(A') = 1.0 \pm 0.15$. Similar results are obtained from the B ← X system. Here, Q and P/R lines are associated with the $\Pi(A')$ and $\Pi(A'')$ Λ-doublet components, respectively.[42,43,45] Thus, the results are susceptible to detection biases and saturation. However, using the instrumental correction factor described in section III.2, the results of the two determinations are identical, within experimental error, as shown in Figure 9, and in Table I. The slight preference for the $\Pi(A')$ component observed for $N'' > 10$ is smaller than that observed by Jursich and Wiesenfeld and is within the precision of our measurements. The Λ-doublet propensities for the CH($X^2\Pi$) obtained in reaction 2 were determined in a similar manner and are shown in Figure 10. They also yield $\Pi(A'')/\Pi(A') \cong 1$; however, as noted above, they may include contributions from other processes.

IV. Discussion

1. Production of C(^{1}D). The production of C(^{1}D) from C_3O_2 by two-photon dissociation at 280 nm has been directly observed via LIF,[24] and the dissociation at 248 nm proceeds via the same electronic transition as the one accessed at 280 nm.[15,37,46,47] Energetically, at these wavelengths carbon atoms cannot be produced by one-photon dissociation, since the formation of C(^{3}P) is possible only below 206.6 nm and that of C(^{1}D), below 171

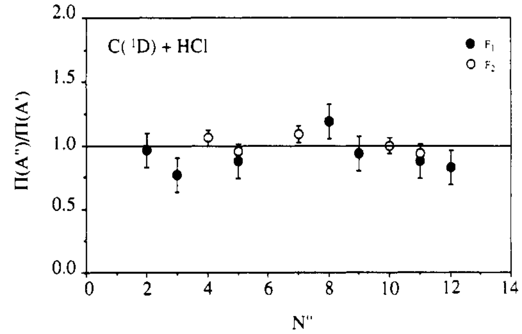

Figure 10. Λ-doublet population ratios obtained in the C(^{1}D) + HCl reaction. The symbols have the same meaning as in Figure 9.

nm.[15,37] The 248-nm band, however, can act as an intermediate in a two-photon process, provided the dissociation

$$C_3O_2 \xrightarrow{248\ \text{nm}} C_2O + CO \qquad \Delta H = 30\,240\ \text{cm}^{-1} \qquad (6)$$

is not too fast. Alternatively, C_2O formed in reaction 6 can absorb an additional photon and dissociate.

The one-photon dissociation of C_3O_2 at 248 nm has recently been studied in detail.[21-23] The main dissociation pathway, reaction 6, appears to proceed from a bent upper state that correlates linearly with the $^1\Pi$ state of C_3O_2 and to CO($X^1\Sigma^+$) + C_2O($\tilde{c}^1\Pi$).[31] However, there is still uncertainty as to which electronic states of C_2O are formed in the one-photon dissociation, and the $\tilde{X}^3\Sigma^-$,[21,22,48-50] $\tilde{a}^1\Delta$,[21,46] and $\tilde{c}^1\Pi$[31] states have all been implicated. Upon collisional relaxation, $C_2O(\tilde{X}^3\Sigma^-)$ has been observed via LIF, whereas no LIF signals are observed under nascent conditions.[49,50] Thus, collision-induced intersystem crossing and/or vibrational relaxation must occur prior to the observation of $C_2O(\tilde{X}^3\Sigma^-)$ in its ground vibrational state. It appears, therefore, that C_2O with substantial internal excitation is produced in the one-photon 248-nm dissociation of C_3O_2.

At pulse energies of 5–10 mJ, C(^{3}P) is produced via a two-photon process, and a ratio C(^{3}P)/CO = 4 ± 2% has been measured.[21] At higher fluences (e.g., focused 150 mJ/pulse), the higher excited states of carbon, C(^{1}S) and C(^{1}D), are produced as well via two-photon processes.[23] The question of sequential vs direct formation of C(^{1}D) at 248 nm is not yet settled, since the UV electronic absorption spectrum of C_2O is unknown, especially when C_2O is formed electronically and/or vibrationally excited.

The two-photon dissociation of C_3O_2 at 248 nm yields C(^{1}D), as well as excited (vibrationally and/or electronically) C_2O, C(^{3}P), and C(^{1}S).[23] It is therefore important to compare our results of reaction 1 with those obtained following 157-nm photolysis of C_3O_2. In the latter process, the major photolysis products are C(^{3}P) and CO($X^1\Sigma$).[31] However, Strauss et al. found that C(^{1}D) is produced in 3% of the dissociation events and is born with 1160 cm^{-1} translational energy (the available energy is 4870 ± 350 cm^{-1}).[31] The reaction of C(^{3}P) with H_2 is endothermic, and the c.m. translational energy is insufficient to overcome the endothermicity for both 157-nm and two-photon 248-nm photolyses. The reaction of C(^{1}S) with H_2 is very slow ($k = \leq 4 \times 10^{-14}$ cm^3 molecule^{-1} s^{-1})[37] and is not expected to contribute significantly to the observed CH signal obtained at low pressures and short delays. The CH rotational distributions obtained via reaction 1 following photolysis of C_3O_2 at 157 and 248 nm are very similar. Thus, we are confident that the major reactant in our experiments is C(^{1}D). With two-photon excitation at 248 nm, the available energy for reaction 1 is ~22 000 cm^{-1}, and assuming a similar ratio of C(^{1}D) translational to available energy, we estimate that the translational energy of C(^{1}D) is likely to be around 5000 cm^{-1}.

(45) Herzberg, G. *Spectra of Diatomic Molecules*; Van Nostrand: New York, 1950.
(46) (a) Bayes, K. D. *J. Am. Chem. Soc.* **1963**, *85*, 1730. (b) Willis, C.; Bayes, K. D. *J. Phys. Chem.* **1967**, *71*, 3367. (c) Bayes, K. D., private communication, 1991.
(47) (a) Roebber, J. L.; Larrabee, J. C.; Huffman, R. E. *J. Chem. Phys.* **1967**, *46*, 4594. (b) Roebber, J. L. *J. Chem. Phys.* **1971**, *54*, 4001.
(48) (a) Becker, K. H.; Horie, O.; Schmidt, V. H.; Wieser, P. *Chem. Phys. Lett.* **1982**, *90*, 64. (b) Bauer, W.; Heuser, R.; Becker, K. H. *J. Photochem.* **1984**, *24*, 2839.
(49) Pitts, W. M.; Donnelley, V. M.; Baronavski, A. P.; McDonald, J. R. *Chem. Phys.* **1981**, *61*, 451, 465.
(50) Donnelley, V. M.; Pitts, W. M.; McDonald, J. R. *Chem. Phys.* **1980**, *49*, 289.

We note, however, that no direct measurements are available to support this estimate.

Before closing, an evaluation of the two-photon photolysis of C_3O_2 at 248 nm as a source of $C(^1D)$ is valuable. The main advantage provided by this method, as compared with 157-nm photolysis, is that fewer reactants absorb or dissociate at 248 nm than at 157 nm. Thus, a larger variety of reactions can be studied. As with 157-nm photolysis, $C(^3P)$ is the major carbon species, and therefore its reactions with the other reactant must be forbidden or much slower. The two-photon 248-nm process is relatively efficient, and the CH signals from reaction 1 are much larger than with, for example, two-photon photolysis at 308 nm.[51] Thus, in principle, adequate signals can be obtained under single-collision conditions, when the observed species is a major reaction product. However, even under these conditions, prompt fluorescence produced in the photolysis of C_3O_2 prevented us from using delays <0.5 μs for CH and CCl detection.

The main uncertainty in using 248-nm photolysis is the role of electronically and/or vibrationally excited C_2O. The one-photon dissociation at 248 nm definitely produces internally excited C_2O.[21,22,48-50] Although ground-state C_2O is not very reactive,[49,50] the metastable $C_2O(\tilde{a}\,^1\Delta)$ has been implicated in reactions.[15,36,46] Singlet C_2O has never been directly observed, but the energies of its low-lying states have been calculated.[52] Thus, experimental tests should be performed to eliminate C_2O as a potential reactant. In our experiments, the dependences on photolysis laser intensity of the CH and CCl signals produced in reactions 1 and 2, respectively, indicate that the reactant is produced via two-photon absorption and therefore is not a low-lying state of C_2O produced by one-photon dissociation. Also, comparisons of the results with those obtained for reaction 1 initiated via 157-nm photolysis lead us to conclude that $C(^1D)$ is the major reacting species. When the observed species is a minor product [e.g., CH from reaction 2], even small contributions from minor reactions can interfere, and the use of the two-photon 248-nm photolysis as a source of $C(^1D)$ then becomes questionable. A cleaner source of $C(^1D)$ is clearly required in order to establish definitively the CH rotational excitations produced in reaction 2.

2. $C(^1D) + H_2$ Reaction. The reaction of $C(^1D)$ with H_2 and its deuterated isotopes has been studied in the past with 157-nm photolysis of C_3O_2 as the source of $C(^1D)$. CH(D) rotational populations and Λ-doublet propensities as well as the [CH]/[CD] ratio were determined.[2-4] The rotational distributions obtained by Jursich and Wiesenfeld[2] are "hotter" than those obtained by Fisher et al.[4] and can be well fit by a statistical prior calculation, provided the thermal internal energy of H_2 is included. Our results, obtained with 248-nm two-photon photolysis of C_3O_2, agree well with those of Jursich and Wiesenfeld. The effect of $C(^1D)$ translational energy on the rotational distribution appears to be small. With 157-nm photolysis, the $C(^1D)$ has an average translational energy of 1160 cm^{-1},[31] and the relative c.m. collision energy with H_2 is only 166 cm^{-1}. Either the translational energy is not effectively converted to CH rotation, or the corresponding energy in the 248-nm photolysis system is not too much higher, since the rotational distribution is similar to the one obtained via 157-nm photolysis. Also, as described above, the effect of translational cooling on the rotational distribution is insignificant. The signals, however, decrease strongly upon quenching of $C(^1D)$ by Xe.

Within our experimental uncertainty, the $CH(X^2\Pi)$ Λ-doublet components for $N'' = 2$–12 are equally populated. The same results are obtained whether the $B \leftarrow X$ or the $A \leftarrow X$ transitions are used. The results for $N'' = 4$–7 are in agreement with those obtained by Jursich and Wiesenfeld,[3] whereas for $N'' > 7$ we still observe a $\Pi(A'')/\Pi(A') = 1.0 \pm 0.15$ (see Figure 3 and Table I), while Jursich and Wiesenfeld obtain ratios 1.0–1.5. Notice also in Figure 3 that R_1 lines are slightly larger than R_2 lines, but when the line strengths for $N'' = J'' + {}^1/_2$ and $J'' - {}^1/_2$ are employed, the line intensities yield equal CH $^2\Pi_{1/2}$ and $^2\Pi_{3/2}$ populations. The absence of a clear preference for the $\Pi(A')$ component contrasts with the observation of large $\Pi(A')/\Pi(A'')$ ratios for $OH(X^2\Pi)$ produced in the reactions of $O(^1D)$ with H_2 and HCl, where ratios up to 3.5 have been observed.[19,44] The $O(^1D) + H_2$ reaction is thought to proceed via an $H_2O(\tilde{X}\,^1A_1)$ intermediate, and the singly occupied π orbital of OH derives from the in-plane bonding H–OH orbital of the planar intermediate.[44,53] In H_2O, the $\tilde{X}\,^1A_1$ state is much lower in energy than the first triplet and excited singlet states, and no barrier exists in the entrance channel. Thus, large attractive forces are expected in the entrance channel which direct the reaction via the $H_2O(\tilde{X}\,^1A_1)$ ground state.[53]

The situation is different in the $C(^1D) + H_2$ system. Here, in analogy with the $O(^1D)$ reaction, a $CH_2(\tilde{a}\,^1A_1)$ intermediate is probably involved, giving rise preferentially to the $\Pi(A')$ $CH(X^2\Pi)$ component. However, two other surfaces are close in energy; the equilibrium energy of the $\tilde{a}\,^1A_1$ surface is only 3165 cm^{-1} above the ground $\tilde{X}\,^3B_1$ state, while the $\tilde{b}\,^1B_1$ surface lies only 10 255 cm^{-1} above the $\tilde{a}\,^1A_1$ surface.[54] These low-lying surfaces can provide attractive interactions in the entrance channel which may be comparable to that of the $\tilde{a}\,^1A_1$ state. The $^{1,3}B_1$ states have unpaired electrons in the b_1 orbital, which is perpendicular to the CH_2 plane, and therefore may yield CH in a $\Pi(A'')$ state.[55] Although the spin selection rules dictate that the entrance approach is along the singlet surfaces, very strong mixings and perturbations are known to exist between the $\tilde{X}\,^3B_1$, $\tilde{a}\,^1A_1$, and $\tilde{b}\,^1B_1$ surfaces of CH_2.[56,57] The mixing matrix elements even at low energies can be >1 cm^{-1}. In fact the authors of ref 56 conclude that spin–orbit couplings mix singlet and triplet wave functions to such an extent that their kinetics cannot be treated separately. In addition, the $\tilde{b}\,^1B_1$ state is coupled to the $\tilde{a}\,^1A_1$ state via Renner–Teller and Coriolis interactions and, indirectly, also to the $\tilde{X}\,^3B_1$ state.[57] Both $^1A_1$ and $^1B_1$ states correlate with the $^1\Delta$ state in the linear configuration, and the large bending amplitudes generated in the intermediate complex certainly provide the transient linear configurations required for efficient mixings.[58,59]

3. $C(^1D)$ + HCl Reaction. Reaction 2 has two channels of comparable exothermicity, one leading to $CH(X^2\Pi)$ and the other to $CCl(X^2\Pi)$. Unfortunately, the heat of formation of CCl is not well known, 120 ± 5 kcal mol^{-1},[15-17] leading to a comparatively large uncertainty in the energetics of reaction 2c. Our experiments indicate that reaction 2c is the major reactive channel. This conclusion is based qualitatively on the observation of large $CCl(X^2\Pi)$ LIF signals, and quantitatively on the ratio of CH obtained from reactions 1 and 2 at similar pressures and delays. In making this comparison, we assume that the rates of the two reactions are similar, as well as the rates of deactivation of $C(^1D)$ to $C(^3P)$. Although the rate of removal of $C(^1D)$ by HCl has not been measured, the rates of the corresponding reactions of $O(^1D)$ are fast and similar (1.3×10^{-10} cm^3 molecule^{-1} s^{-1} for H_2 and 1.5×10^{-10} cm^3 molecule^{-1} s^{-2} for HCl).[60,61] The rate of removal of $C(^1D)$ by H_2, $(0.4–2.6) \times 10^{-10}$ cm^3 molecule^{-1} s^{-1},[37] is similar to those of the corresponding $O(^1D)$ reactions, and therefore we assume that the rate of reactions 2 is of the same magnitude. Another implicit assumption is that reactions 1 and 2 are the predominant deactivation channels of $C(^1D)$ rather than physical quenching to $C(^3P)$. This again is analogous to with the corresponding situation with $O(^1D)$.[18,61] However, the possible mixings between triplet and singlet CH_2(CHCl) states may encourage quenching of $C(^1D)$ to $C(^3P)$ via a carbene intermediate. On the

(51) de Juan, J.; Reisler, H., unpublished work.
(52) Walch, S. P. *J. Chem. Phys.* **1980**, *72*, 5679.
(53) Sloan, J. J. *J. Phys. Chem.* **1988**, *92*, 18, and references cited therein.
(54) Jacox, M. E. *J. Phys. Chem. Ref. Data* **1988**, *17*, 269.
(55) Gaspar, P. P.; Hammond, G. S. In *Carbenes*; Moss, R. A., Jones, M. Jr., Eds.; Wiley: New York, 1975; Vol. II, p 204.
(56) Petek, H.; Nesbitt, D. J.; Moore, C. B.; Birss, F. W.; Ramsay, D. A. *J. Chem. Phys.* **1987**, *86*, 1189.
(57) Petek, H.; Nesbitt, D. J.; Darwin, D. C.; Moore, C. B. *J. Chem. Phys.* **1987**, *86*, 1172.
(58) Shavitt, I. *Tetrahedron* **1985**, *41*, 1531.
(59) Schaefer, H. F. III. *Science* **1986**, *231*, 1100.
(60) Davidson, J. A.; Sadowski, C. M.; Shiff, H. I.; Howard, C. J.; Jennings, D. A.; Schmeltekopf, A. L. *J. Chem. Phys.* **1976**, *64*, 53.
(61) Wine, P. J.; Wells, J. H.; Ravishankara, A. R. *J. Chem. Phys.* **1986**, *84*, 1349.

basis of these assumptions we place a lower limit $[CH(H_2)]/[CH(HCl)] \geq 7$. Since twice as much CH can be produced in reaction 1 as in reaction 2, we estimate that $k(1)/k(2a,b) \geq 4$. The lower limit reflects the fact that there is some contamination in the CH signals from reaction 2 as discussed above.

The $CCl(A^2\Delta \leftarrow X^2\Pi)$ spectra displayed in Figure 6 show a large degree of rotational excitation. The spectrum obtained at 1.0 μs delay appears more relaxed than that taken at 0.5 μs delay indicating that the data at long time delays are affected by relaxation. However, spectra taken at 0.2 μs delay do not show significantly higher excitation than at 0.5 μs delay [i.e., the (0,0) P_1 bandhead is not significantly larger], indicating that near nascent conditions are reached. However, the S/N at the very short delay times is rather poor because of the large fluorescence background. In the simulations shown in Figure 7 we used Boltzmann populations, truncated at $N'' = 100$, and varied the temperatures. We emphasize that there is no justification for using temperatures, except that the large degree of spectral overlap renders the simulations insensitive to the exact shape of the rotational distribution, and thus does not warrant the use of more elaborate distribution functions. As mentioned above, the data can be well simulated by assuming $E_{rot} = 1700$–2500 cm^{-1}.

Reaction 2 generates CH and CCl with high rotational excitation, suggesting an insertion mechanism with predominantly perpendicular approach. In particular, the P_1 bandhead of CCl is formed by rotational levels $N'' > 45$ which are near the thermochemical limit. Notice also that because of the mass ratios, the 5000-cm^{-1} translational energy of $C(^1D)$ estimated above leads to a c.m. collision energy of 3800 cm^{-1}, which is significant. The importance of the relative translational energy could not be assessed experimentally, because at the pressures requisite for translational cooling the $CCl(X^2\Pi)$ rotational distribution starts to relax, and the contributions of translational deactivation and rotational relaxation cannot be separated.

The CCl LIF spectra show peaks that indicate the formation of CCl in $v'' = 0$–3. Although the lack of accurate spectroscopic information prevents us from evaluating exactly the vibrational distribution, it is clear that $v'' = 0,1 > v'' = 2,3$, no population inversion exists, and both $v'' = 0$ and 1 are significantly populated. In fact, simulations assuming $n(v''=1)/n(v''=0) \cong 3/4$ and $T = 3000$ K yield reasonable agreement with the measured spectra as evident from Figures 6 and 7. Thus, the CCl product shows substantial vibrational and rotational excitation.

4. Reaction Mechanisms: Comparisons with $O(^1D)$ Reactions. The reactions of $C(^1D)$ show clear similarities with those of $O(^1D)$. The electronic configurations of the two atoms are similar in that both have two unpaired electrons in p orbitals, and the only difference is that $O(^1D)$ has, in addition, one filled p orbital. While little is known about the reactions of $C(^1D)$, the reactions of $O(^1D)$ have been thoroughly investigated, both experimentally and theoretically. It appears that the reactions of $O(^1D)$ with H_2 (HCl) involve an insertion mechanism and proceed via HOH(Cl) intermediates.[18,19,44,53,62-64] The reactions apparently involve the ground electronic surface of HOH(Cl) with no entrance barrier and lead to high OH rotational and vibrational excitations. Trajectory calculations indicate that the HOH and HOCl intermediates probably live only for few vibrational periods, a time too short for complete energy randomization.[53,62-64] Fitzcharles and Schatz have shown that while the calculated $OH(X^2\Pi)$ rotational distributions from $O(^1D) + H_2$ look statistical, they do not agree exactly with phase space calculations.[62] The high rotational excitations arise predominantly from repulsions between the two hydrogen atoms when the H_2O complex breaks up. Substantial vibrational excitation also results, which depends on the details of the PES in a subtle way. Sloan and his co-workers carried out trajectory calculations for this reaction and showed that, after traversing the HOH minimum, the system executes an inversion in the bending vibrational mode before finally dissociating into products.[53]

We suggest that the $C(^1D) + H_2$ reaction proceeds through a similar insertion mechanism with two notable differences. The exothermicity of the reaction is substantially smaller, thereby precluding vibrational excitation in CH, and the availability of low-lying $^3B_1$ and $^1B_1$ surfaces, which are known to couple efficiently to the $^1A_1$ surface,[56,57] encourages reactions on more than one surface. For example, the large-amplitude bending motion that leads to inversion must proceed through the linear configuration where the Renner–Teller $^1A_1$ and $^1B_1$ states are degenerate.[58,59] As described above, the mixings with surfaces of B_1 symmetry may explain the absence of Λ-doublet preference in $CH(X^2\Pi)$, in contrast with the $O(^1D) + H_2$ reaction, which shows a distinct preference of the $\Pi(A')$ Λ-doublet component of $OH(X^2\Pi)$.

The reaction of $C(^1D) + H_2$ has been studied theoretically by Blint and Newton, who performed ab initio CI calculations on the $C(^3P,^1D) + H_2$ system.[65] These authors found no barrier for $C(^1D)$ insertion via the $^1A_1$ surface of CH_2, but showed that a barrier to linear abstraction does exist. In contrast, the $C(^3P)$ insertion via $CH_2(\tilde{X}^3B_1)$ shows a substantial barrier in the entrance channel. However, in the vicinity of the $^3B_1$ barrier, the $^3A_2$ state, which lies at much higher energies at the equilibrium CH_2 geometry, has a much lower energy. In C_s configuration, the $^3B_1$ and $^3A_2$ states both become A'', and the avoided crossing lowers the barrier height substantially. In fact, in a later publication, Harding found a barrier height ≤ 1 kcal/mol, even though the insertion reaction is forbidden by the Woodward–Hoffmann rules.[66] Thus, in the $C(^3P) + H_2 \rightarrow CH_2$ reaction, either the $^3B_1$ or the $^3A_2$ state of CH_2 may be formed. Likewise, in the $C(^1D) + H_2$ reaction, the $^1A_1$, $^1B_1$, and 2^1A_1 states may participate. We assume, based on spin-selection rules, that the initial approach is along the singlet surfaces, but there is no theoretical reason why efficient couplings to the triplet surfaces would not play an important role.

The $O(^1D)$ + HCl reaction was studied with both vibrational and rotational resolution.[18,19] OH is the major product, since the exothermicity of this channel (−44.5 kcal/mol) is much larger than for the OCl channel (−6 kcal/mol). Again, the reaction is thought to proceed via the $HOCl(^1A')$ intermediate[18] and yields a distinct preference for the $\Pi(A')$ Λ-doublet component of $OH(X^2\Pi)$.[19] High rotational populations are obtained, which are nonstatistical, and the vibrational distribution is inverted.[18,19] Although the OH product distributions resemble those obtained via abstraction, the authors favor an insertion mechanism with a short-lived intermediate.[19] The H–Cl repulsion is the predominant source of the OH excitations, and quenching of $O(^1D)$ happens in only about 5% of the collisions.[18] Very recent results on the OCl fragment yield a ratio $[OCl]/[OH] \sim 0.36$, much greater than anticipated on statistical grounds.[61,67] The possibility that some of the OCl product arises via abstraction involving an HClO PES has been raised.[67]

The $C(^1D)$ + HCl reaction is also likely to proceed via an insertion mechanism, since we observe rotational and vibrational excitation in the products up to (and even above) the thermochemical limit. The large propensity for formation of CCl, as opposed to CH, is probably a result of the H–Cl repulsion; the rapidly moving H is more likely to depart, while the slow moving Cl forms the bond with C. This may also account for the larger CD population observed in the $C(^1D)$ + HD reaction.[4] The H–Cl repulsion may also be the cause of the substantial CCl internal excitation, while the proximity of singlet and triplet states of A'' symmetry of the HCCl intermediate may promote couplings and result in equal populations of Λ-doublets. Ab initio calculations by Scuseria et al.[68] place the singlet–triplet separation in HCCl

(62) Fitzcharles, M. S.; Schatz, G. C. *J. Phys. Chem.* **1986**, *90*, 3634.
(63) Badenhoop, J. K.; Koizumi, H.; Schatz, G. C. *J. Chem. Phys.* **1989**, *91*, 142.
(64) Goldfield, E. M.; Wiesenfeld, J. R. *J. Chem. Phys.* **1990**, *93*, 1030.
(65) Blint, R. J.; Newton, M. D. *Chem. Phys. Lett.* **1975**, *32*, 178.
(66) Harding, L. B. *J. Phys. Chem.* **1983**, *87*, 441.
(67) Balucani, N.; Beneventi, L.; Casavecchia, P.; Volpi, G. G. *Chem. Phys. Lett.* **1991**, *180*, 34.
(68) Scuseria, G. E.; Durán, M.; Maclagan, G. A. R.; Schaefer, H. F. III. *J. Am. Chem. Soc.* **1986**, *108*, 3248.

at 1900 cm^{-1}, while the observed origin of the $\tilde{A}^1A''$ state is at 12274 cm^{-1},[54] well below the C(^{1}D) + HCl entrance energy. Nevertheless, the participation of an abstraction mechanism cannot be ruled out and calculations are clearly needed to sort out the contributions of the different mechanisms.

V. Summary

The reactions of C(^{1}D) with H_2 and HCl were studied using two-photon photolysis of C_3O_2 at 248 nm as the source of C(^{1}D). Both reactions give rise to products (CH, CCl) with high internal excitation. CCl is the major diatomic product in the C(^{1}D) + HCl reaction, even though the reaction channel yielding CH has comparable exothermicity.

The internal state distributions in the products can be rationalized by an insertion mechanism with short-lived carbene intermediates (i.e., CH_2, CHCl). The initial, spin-allowed approach is along the $\tilde{a}^1A_1$ or $\tilde{X}^1A'$ singlet surfaces of HCH(Cl), but the participation of higher singlet surfaces is also possible. The existence of low-lying triplet states, Renner–Teller pairs, Coriolis couplings, and large spin–orbit matrix elements provides many opportunities for subsequent surface crossings, aided by strong bending motions in the intermediate, and both singlet and triplet surfaces may participate in the reactions. The participation of surfaces of B_1 or A'' symmetry in the reactions with H_2 and HCl, respectively, may account for the absence of significant Λ-doublet preferences in the CH($X^2\Pi$) product. In general, the insertion mechanism is analogous to the mechanism of the corresponding O(^{1}D) reactions, and calculations indicate that abstraction has a substantial barrier. In further analogy with O(^{1}D) reactions, the reactive intermediate is likely to be short-lived, and the large degree of product internal excitation derives from H–H or H–Cl repulsions. Better potential energy surfaces and dynamical calculations are clearly needed to aid in determining the importance of the different possible mechanisms.

Acknowledgment. We thank S. Reid, F. Winterbottom, C. X. W. Qian, and S. Sharpe for illuminating discussions and help in the computer simulations, and Kevin Shannon for his enthusiastic technical help. We are grateful to I. Burak for communicating to us, prior to publication, the improved procedure for C_3O_2 synthesis. Support by the Chemical Sciences Division of the Office of Basic Energy Sciences, U.S. Department of Energy, is gratefully acknowledged. D.C.S. thanks the Department of Education for a graduate student fellowship.

Registry No. C_3O_2, 504-64-3; C, 7440-44-0; H_2, 1333-74-0; HCl, 7647-01-0; CH, 3315-37-5; CCl, 3889-76-7; CH_3I, 74-88-4; Xe, 7440-63-3.

Temperature-Dependent Kinetics Studies of the Reactions Br($^2P_{3/2}$) + H_2S ↔ SH + HBr and Br($^2P_{3/2}$) + CH_3SH ↔ CH_3S + HBr. Heats of Formation of SH and CH_3S Radicals

J. M. Nicovich, K. D. Kreutter, C. A. van Dijk, and P. H. Wine*

Physical Sciences Laboratory, Georgia Tech Research Institute, Georgia Institute of Technology, Atlanta, Georgia 30332 *(Received: August 5, 1991)*

Time-resolved resonance fluorescence detection of Br($^2P_{3/2}$) atom disappearance or appearance following 266-nm laser flash photolysis of $CF_2Br_2/H_2S/H_2/N_2$, $CF_2Br_2/CH_3SH/H_2/N_2$, $Cl_2CO/H_2S/HBr/N_2$, and $CH_3SSCH_3/HBr/H_2/N_2$ mixtures has been employed to study the kinetics of the reactions Br($^2P_{3/2}$) + H_2S ⇄ SH + HBr (1, −1) and Br($^2P_{3/2}$) + CH_3SH ⇄ CH_3S + HBr (2, −2) as a function of temperature over the range 273–431K. Arrhenius expressions in units of 10^{-12} cm^3 molecule^{-1} s^{-1} which describe the results are $k_1 = (14.2 \pm 3.4)\exp[(-2752 \pm 90)/T]$, $k_{-1} = (4.40 \pm 0.92)\exp[(-971 \pm 73)/T]$, $k_2 = (9.24 \pm 1.15)\exp[(-386 \pm 41)/T]$, and $k_{-2} = (1.46 \pm 0.21)\exp[(-399 \pm 41)/T]$; errors are 2σ and represent precision only. By examining Br($^2P_{3/2}$) equilibration kinetics following 355-nm laser flash photolysis of $Br_2/CH_3SH/H_2/N_2$ mixtures, a 298 K rate coefficient of $(1.7 \pm 0.5) \times 10^{-10}$ cm^3 molecule^{-1} s^{-1} has been obtained for the reaction $CH_3S + Br_2 \rightarrow CH_3SBr + Br$. To our knowledge, these are the first kinetic data reported for each of the reactions studied. Measured rate coefficients, along with known rate coefficients for similar radical + H_2S, CH_3SH, HBr, Br_2 reactions are considered in terms of possible correlations of reactivity with reaction thermochemistry and with IP − EA, the difference between the ionization potential of the electron donor and the electron affinity of the electron acceptor. Both thermochemical and charge-transfer effects appear to be important in controlling observed reactivities. Second and third law analyses of the equilibrium data for reactions 1 and 2 have been employed to obtain the following enthalpies of reaction in units of kcal mol^{-1}: for reaction 1, $\Delta H_{298} = 3.64 \pm 0.43$ and $\Delta H_0 = 3.26 \pm 0.45$; for reaction 2, $\Delta H_{298} = -0.14 \pm 0.28$ and $\Delta H_0 = -0.65 \pm 0.36$. Combining the above enthalpies of reaction with the well-known heats of formation of Br, HBr, H_2S, and CH_3SH gives the following heats of formation for the RS radicals in units of kcal mol^{-1}: $\Delta H_f{}^\circ{}_0(SH) = 34.07 \pm 0.72$, $\Delta H_f{}^\circ{}_{298}(SH) = 34.18 \pm 0.68$, $\Delta H_f{}^\circ{}_0(CH_3S) = 31.44 \pm 0.54$, $\Delta H_f{}^\circ{}_{298}(CH_3S) = 29.78 \pm 0.44$; errors are 2σ and represent estimates of absolute accuracy. The SH heat of formation determined from our data agrees well with literature values but has reduced error limits compared to other available values. The CH_3S heat of formation determined from our data is near the low end of the range of previous estimates and is 3–4 kcal mol^{-1} lower than values derived from recent molecular beam photofragmentation studies.

Introduction

Accurate thermochemical information for free-radical intermediates is essential to analysis of reaction mechanisms in complex chemical systems. One experimental approach which can be employed to obtain thermochemical parameters for a radical R involves measurement of temperature-dependent rate coefficients for the pair of reactions RH + R′ ↔ R′H + R; the ideal reaction pair for such a study is one where the heats of formation and absolute entropies of R′, R′H, and RH are well characterized and where kinetic data for the two reactions can be obtained over the same temperature range.

In this paper we report the results of temperature-dependent kinetics studies of the following four reactions:

$$Br(^2P_{3/2}) + H_2S \rightarrow SH + HBr \quad (1)$$

$$SH + HBr \rightarrow Br(^2P_{3/2}) + H_2S \quad (-1)$$

$$Br(^2P_{3/2}) + CH_3SH \rightarrow CH_3S + HBr \quad (2)$$

$$CH_3S + HBr \rightarrow Br(^2P_{3/2}) + CH_3SH \quad (-2)$$

* Author to whom correspondence should be addressed.

